POLITECNICO DI TORINO
Repository ISTITUZIONALE

Ageing effects on the linear and nonlinear viscoelasticity of bituminous binders

(Article begins on next page)

17 April 2024

Ageing effects on the linear and nonlinear viscoelasticity of bituminous binders

Tsantilis Lucia [a]*, Underwood B. Shane [b], Miglietta Fabrizio [a], Riviera Pier Paolo [a],

Baglieri Orazio [a] and Santagata Ezio [a].

[a] *Department of Environment, Land and Infrastructure Engineering, Politecnico di Torino, Torino, Italy;*

[b] *Department of Civil, Construction, and Environmental Engineering, North Carolina State University, Raleigh, NC, USA.*

**lucia.tsantilis@polito.it*

The paper investigates the effects of ageing on the linear and nonlinear viscoelastic properties of bituminous binders for paving applications. Four neat binders were analysed in their unaged state and after long-term ageing, which was simulated in the laboratory with the Rolling Thin Film Oven (RTFO) and the Pressure Ageing Vessel (PAV). Amplitude sweep tests and frequency sweep tests were performed to explore the response in the linear domain. Repeated strain sweep tests were carried out to isolate nonlinearity from other mechanisms related to damage. The time-temperature superposition principle and the generalized Maxwell model with a Prony series discretization were used to describe the overall viscoelastic response of binders, introducing strain-dependent shift factors to account for nonlinearity. Results indicate that the adopted experimental and modelling approach allows a proper assessment of the effects of ageing on viscoelasticity.

Keywords: bituminous binders; viscoelasticity; nonlinearity; chemical ageing

Introduction

Chemical ageing is one of the most important phenomena impacting on the overall properties of bituminous binders. It stems from the combined progression of several chemical reactions and physical processes that yield permanent changes in the molecular structure of bitumen. These are generally grouped into oxidation reactions, polymerization, and evaporation of volatile components. Oxidation leads to an increase in polar chemical functionalities containing oxygen such as sulfoxides, anhydrides, ketones and carboxylic acids, that, in turn, can promote molecule condensation mechanisms as a consequence of their highly interacting features (Petersen, 1986). The contribution provided by evaporation is generally more limited than that related to oxidation

and polymerization. This difference is mainly due to the possibility, at the refining stage, to effectively control the amount of volatile components with the twofold objective of increasing the efficiency of light fraction extraction and reducing toxic fumes that can be generated during hot mix asphalt production and paving operations. Given the strong dependency of the kinetics of ageing on temperature, a distinction is made between the so-called short-term and long-term chemical ageing. Short-term ageing refers to the rapid process that is triggered by the high temperatures involved during hot mix production, transportation, laying and compaction. Long-term ageing is related to the progressive ageing that takes place during the prolonged period of time the pavement surface is exposed to the atmosphere at in-service temperatures (Tauste et al., 2018). Numerous methods have been proposed to simulate, in the laboratory, the mechanisms of ageing occurring in bitumen during actual paving applications (Hofko et al., 2018; Mirwald et al., 2020; Sun et al., 2020). The most common standardized protocols are based on the use of the Rolling Thin Film Oven (RTFO) and the Pressure Ageing Vessel (PAV) tests (Airey, 2003).

It is widely recognized that the permanent changes occurring in bitumen microstructure can negatively affect the durability of asphalt pavements and lead to premature failures, as demonstrated by several studies which investigated the performance-related properties of both fracture and fatigue resistance (Glover et al., 2009; Walubita et al., 2006). From a rheological point of view, a shift towards a more solid-like behaviour is commonly revealed after ageing, as indicated by the increase in stiffness and elasticity typically exhibited in the linear viscoelastic domain (Lu & Isacsson, 2002). Extending the analysis to the nonlinear domain, Masad and co-workers (2008) combined stress-dependent shift factors with specific ageing shift factors to describe the overall viscoelastic properties of binders, finding that the ageing shift factors were independent of the stress level but dependent upon temperature. Rahmani et al. (2017) proposed a coupled ageing-viscoelastic constitutive relationship based on the use of an ageing state variable to predict the nonlinear viscoelastic response of mixtures at different stress levels, air void contents, and temperatures.

The study presented in this paper investigated the effect of chemical ageing on the rheology of bitumen. The time-temperature superposition principle and the generalized Maxwell model with a Prony series discretization were used to depict the viscoelastic properties of the binders introducing strain-dependent shift factors to account for nonlinearity.

Materials and methods

Materials characterization

Four neat bituminous binders were analysed, coded as A, B, C, and D. In order to maximize the variability in bitumen structure and composition, the four binders were obtained from different refineries, located in France (bitumen A), in Italy (B), and in the United States of America (C and D).

All materials were tested in both unaged and long-term aged conditions. Ageing was simulated in the laboratory by first subjecting the virgin bitumen to the Rolling Thin Film Oven (RTFO) test (as per AASHTO T 240) and by then subjecting the RTFO residue to the Pressure Ageing Vessel (PAV) treatment (at 100 °C for 20 h with 2.1 MPa pressure, as per AASHTO R 28).

Insights into the chemical structure of the four considered binders were gained by means of the SARA analysis, based on the combined use of capillary thin layer chromatography (TLC) and flame ionization detection (FID). While TLC allows separation of bitumen in four fractions based on their solubility and polarity features, FID is needed to quantitatively assess the relative percentages of the separated fractions. The TLC procedure started with the preparation of a bitumen-dichloromethane solution (10 mg of bitumen in 1 ml of dichloromethane). Afterwards, 1 μl of sample solution was spotted on silica rods and oven-dried for two minutes. Silica rods were subjected to three successive elutions in development tanks containing n-hexane, toluene, and a solution of dichloromethane and methanol in a volume ratio of 95:5. Each elution was followed by an oven-drying phase of two minutes to remove the solvent from the rods. FID was carried out by

means of a Iatroscan MK-6 operated with a pure hydrogen flow of 160 ml/min, an air flow of 2 l/min and a scanning speed of 30 s/scan.

Results obtained from SARA analysis for the binders in their unaged (U) and long-term aged (PAV) states are presented in Figure 1, which displays the percentages of Saturates (Sa), Aromatics (Ar), Resins (Re), and Asphaltenes (As). Table 1 lists synthetic microstructural indices: the Colloidal Instability Index (CII) defined as the ratio between the sum of saturates and asphaltenes to the sum of resins and aromatics, the ratio of saturates to aromatics (Sa/Ar), and the ratio of asphaltenes to resins (As/Re).
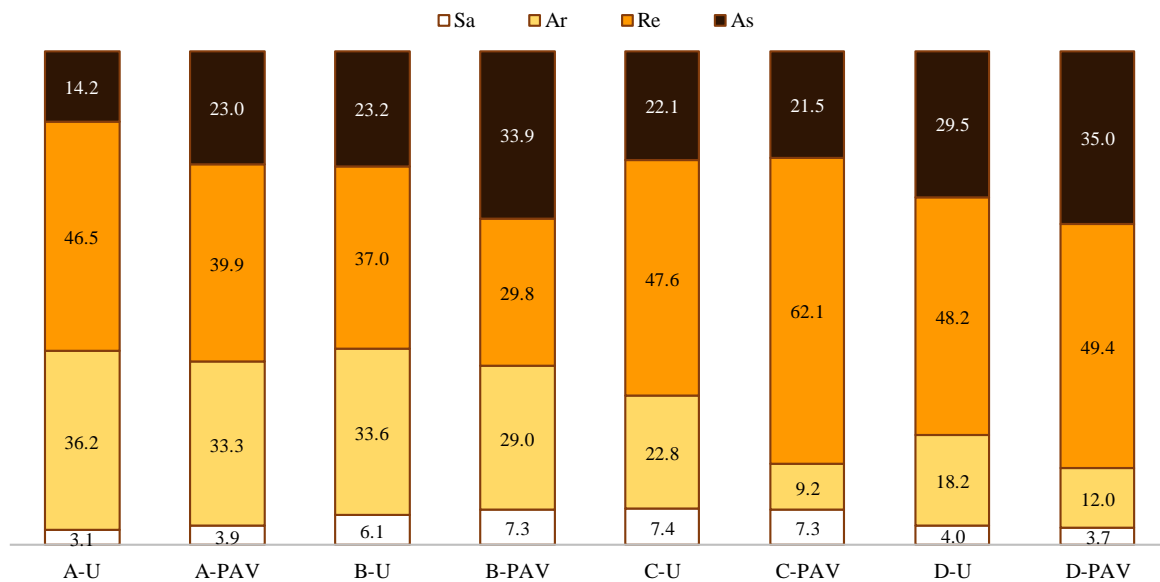

Figure 1. Percentages of Saturates (Sa), Aromatics (Ar), Resins (Re), and Asphaltenes (As).

	A-U	A-PAV	B-U	B-PAV	C-U	C-PAV	D-U	D-PAV
CII	0.209	0.368	0.415	0.700	0.419	0.404	0.505	0.630
Sa/Ar	0.085	0.117	0.181	0.250	0.325	0.792	0.221	0.305
As/Re	0.306	0.577	0.627	1.138	0.464	0.346	0.612	0.708

Table 1. Colloidal Instability Index (CII), ratio of saturates to aromatics (Sa/AR), and ratio of asphaltenes to resins (As/Re).

When considering the four selected binders in their unaged state, significant differences can be noted in the outcomes of fractionation, thus confirming the non-negligible influence of the source and refining process on the microstructure of bitumen (Paliukait et al., 2014).

Analysing the effects of ageing, it can be shown that maximum variations in saturates were found to be around 1 %, thus indicating a lower involvement of this fraction in the overall ageing mechanisms due to its low chemical reactivity (Lesueur, 2009). When considering the other fractions, it is commonly accepted that during ageing, aromatics generate resins that in turn generate asphaltenes (Siddiqui & Ali, 1999; Fallah et al., 2019). However, listed results seem to reflect different ageing patterns followed by the various materials. Binders A and B showed an increase in the content of asphaltenes counterbalanced by a predominant reduction of the resins and a lower reduction of the aromatics. In binder C, asphaltenes remained almost unchanged, while a substantial increase in resins and decrease in aromatics were recorded. On the other hand, bitumen D showed a dramatic drop in aromatics, a substantial growth in asphaltenes and a slight increase in resins.

Rheological measurements

Rheological tests were carried out by means of a Dynamic Shear Rheometer (Anton Paar MCR 302), an air bearing stress-controlled device which can also operate in the strain-controlled mode through a feedback controlled loop. The DSR is equipped with a permanent magnet synchronous drive (minimum torque = 1 nNm) and an optical incremental encoder for measurement of angular rotation (minimum angular deflection 0.05 μrad). An 8-mm parallel plate sensor system was used with a 2-mm gap between the plates. In order to thoroughly investigate the response of the binders in both the small and large amplitude oscillatory shear conditions, three types of tests were considered: strain amplitude sweep, frequency sweep, and repeated strain sweep tests. Strain amplitude sweeps were conducted at first to identify proper input parameters to be used in the linear viscoelastic characterization. Frequency sweep and repeated strain sweep tests were used to explore the linear and nonlinear viscoelastic response of binders, respectively.

Strain amplitude sweep tests were carried out at three temperatures, 4 °C, 15 °C, 34 °C, at angular frequencies of 1 rad/s (for tests at 15 °C and 34 °C) and 100 rad/s (for tests at 4 °C and 15 °C). Depending on the combination of temperature and angular frequency, the strain amplitude was varied in the range comprised between 0.0001 % and 100 %, acquiring 10 points/decade. Frequency sweep tests were performed between 4 °C and 34 °C, at steps of 6 °C. At each temperature, the angular frequency was varied between 1 rad/s and 100 rad/s recording 10 points/decade. Strains belonging to the linear viscoelastic range were selected at each combination of temperature and frequency on the basis of the outcomes of the strain amplitude sweep tests. Repeated strain sweep tests were run at temperatures of 34 °C, 28 °C, 16 °C, and 10 °C at a constant frequency of 10 Hz. This type of test was composed of different phases, indicated in the following as groups (at least two per test) and blocks (three per group). During each group, the strain was raised for three times from an initial to a final value following a logarithmic ramp. While the low initial value of strain was always the same in a test, the final value changed depending on the group. At least two levels of the final strain were selected, one belonging to the linear viscoelastic range and the other to the nonlinear range. Each of the three strain ramps performed in one group was identified as one block.

In order to guarantee a proper achievement of the imposed strain inputs, rheological measurements were all carried out in no-time setting conditions and the test duration was verified to be coherent among different materials. Prior to testing, specimens were allowed to reach thermal equilibrium by using a 35 minutes conditioning phase. A minimum of two replicates were performed for all tests and average values were considered in the analyses.

Results and analysis

Linear viscoelastic properties

In the laboratory characterization of viscoelastic materials, the selection of proper strain or stress inputs to be adopted at each specific testing condition is of primary importance to obtain reliable

experimental outcomes (Airey, 2002). When considering oscillatory tests to investigate the linear viscoelastic response of materials, the strain level must be comprised between an upper limiting value (γ_L), that depends on the frontier of the linear range, and a lower value (γ_0), mainly dictated by instrumental resolution. These extreme strain values can be determined at each temperature and frequency condition by means of strain amplitude sweep tests, during which the variation in rheological parameters can be monitored as a function of increasing strain. This is illustrated in Figure 2a, where the evolution of the norm of the complex modulus $|G^*|$, calculated as the ratio of stress to strain amplitudes, is plotted versus the strain amplitude γ. In order to exclude undesirable noise in data acquisition caused by testing conditions too close to instrumental limits, γ_0 was taken as the smallest strain level when the difference between the relative variations between successive $|G^*|$ and the plateau values of the linear range were lower than 0.5 %. The frontier of the linear viscoelastic domain was taken as the point where the $|G^*|$ was 5 % smaller than the initial value of $|G^*|$.
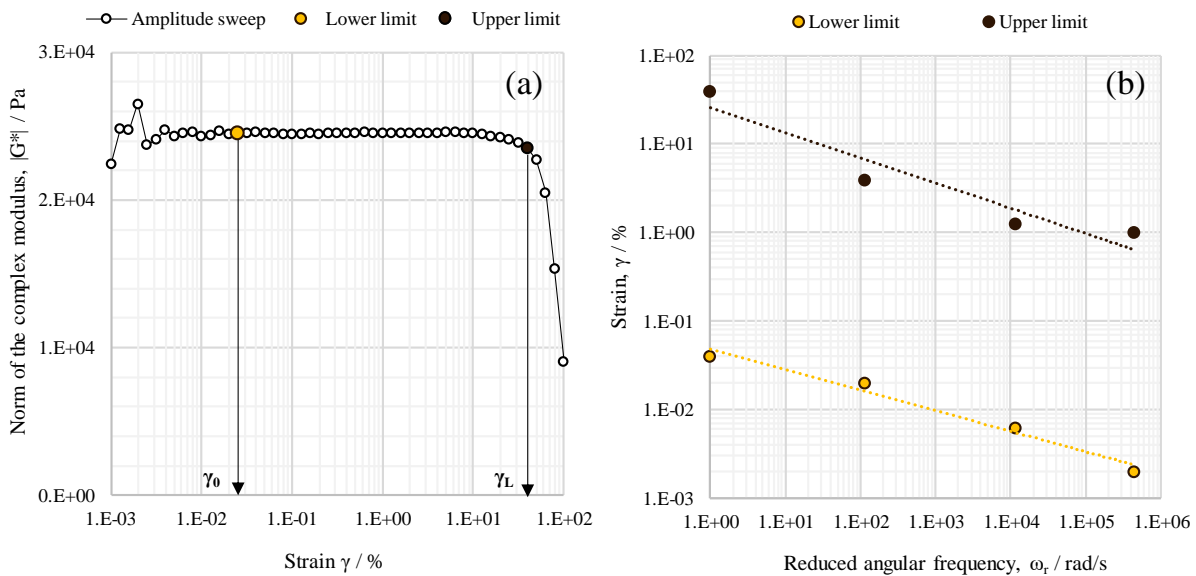

Figure 2. (a) Definition of γ_0 and γ_L in amplitude sweep tests (bitumen A-U at 34 °C and 1 rad/s); (b) Typical plot of γ_0 and γ_L versus ω_r at a reference temperature of 34 °C (bitumen A-U).

Next, strain boundaries were defined as a function of reduced angular frequency ω_r, thus allowing the description of the linearity range as a function of both time and temperature, combined

in a single variable. Moreover, as displayed in Figure 2b, ~~so that~~ the strain limits found in the four conditions directly investigated by means of amplitude sweep tests (4 °C at 100 rad/s, 15 °C at 1 rad/s and 100 rad/s, 34 °C at 1 rad/s) could be extended to all temperature and frequency combinations considered in frequency sweeps. Plots of the lower and upper limiting values of strain as a function of the reduced angular frequency were therefore constructed for all materials and used for the selection of proper strain values to be adopted in the linear viscoelastic characterization. In the calculation of the reduced angular frequency, the physical angular frequency was multiplied by typical shift factor values and then corrected with the experimentally-derived shifts specifically obtained for each material.

From this preliminary characterization performed to identify the linear viscoelastic conditions, it was observed that ageing always induced a general contraction of the linear viscoelastic range. By referring to the fitting curve of the linear relationship between the upper limiting value of strain and the reduced frequency presented in Equation 1, such a contraction can be clearly highlighted by the significant decrease in the intercept and by the slight variation in slope caused by ageing.

$$Log(\gamma_L) = log(a) + b \, Log(\omega_r) \tag{1}$$

Table 2. Regression coefficients of γ_L versus ω_r relationships for all binders.

	A-U	A-PAV	B-U	B-PAV	C-U	C-PAV	D-U	D-PAV
a	26.74	13.80	2.12	1.23	27.13	5.24	10.99	2.65
b	-0.28	-0.24	-0.05	-0.04	-0.29	-0.15	-0.21	-0.10

The linear viscoelastic response of the binders was analysed by modelling the outputs of frequency sweep tests by means of the generalized Maxwell model using a Prony series discretization. This approach, that has the potential to easily interconvert functions between the frequency and time domains, also served as a basis for the subsequent study of nonlinearity.

In order to calculate Prony coefficients, values of the norm and phase angle of the complex modulus were initially modelled in the form of master curves according to the time-temperature

superposition principle. Raw data collected at different temperatures were shifted along the frequency axis, thus defining continuous rheological functions at a reference temperature and conveniently expanding the range of frequencies from those that can be physically measured. Moreover, also with the purpose of pre-smoothing raw data from eventual fluctuations that can cause detrimental effects in the definition of the Prony terms, the construction of master curves was performed by means of an optimization process fitting measured data to the Williams-Landel-Ferry (WLF) (Ferry, 1980) and the Christensen-Anderson-Marasteanu (CAM) (Marasteanu & Anderson, 1999) analytical functions, for the time-temperature shift factors and master curves, respectively. These analytical functions are presented in Equations 2 to 4:

$$Log \; a_T = \frac{-C_1(T - T_R)}{(C_2 + T - T_R)} \tag{2}$$

$$|G^*|_{LVE} (\omega_r) = G_g \left[1 + \left(\frac{\omega_c}{\omega_r} \right)^{\frac{Log \, 2}{R}} \right]^{-\frac{m \, R}{Log \, 2}} \tag{3}$$

$$\delta_{LVE} (\omega_r) = \frac{90 \, m}{\left[1 + \left(\frac{\omega_r}{\omega_c} \right)^{\frac{Log \, 2}{R}} \right]} \tag{4}$$

where in Equation 2 a_T is the time-temperature shift factor between the generic test temperature T and the reference temperature T_R, selected equal to 10 °C in the following analyses, while C_1 and C_2 are fitting constants. In Equation 3 and 4, $|G^*|_{LVE}$ and δ_{LVE} are the norm and the phase angle of the complex modulus, ω_r is the reduced angular frequency, equal to the product between the physical angular frequency ω and the time-temperature shift factor a_T, G_g is the glassy modulus, ω_c, R and m are model parameters. The subscript 'LVE' is added to these variables to indicate that those parameters specifically refer to the linear viscoelastic range.

Prony series were determined by first deriving the Prony coefficients using the collocation method. Given the definition of the relaxation modulus as a function of time $G(t)$ displayed in Equation 5, for a generic n number of elements in the Prony series, G_i represents the ith stiffness term and ρ_i is the corresponding ith relaxation time.

$$G(t) = \sum_{i=1}^{n} G_i \, e^{-t/\rho_i}$$

A set of relaxation times ρ_i and angular frequency ω_k (arbitrarily imposed equal to ρ_i) were selected covering 16 decades of loading time/frequency which always included the interval of reduced frequencies obtained from the shifting of experimental data.

The Prony terms, G_i, were than calculated as indicated in Equation 6:

$$\{G_i\} = [A]^{-1}\{G'\} \tag{6}$$

where $\{G_i\}$ is the array of G_i Prony terms to be determined, $\{G'\}$ is the array of storage moduli (derived from pre-smoothened experimental data at frequencies ω_k as the product between the norm of the complex modulus and the cosine of the phase angle), and [A] is the kernel matrix in which the ith and kth terms were calculated as a function of relaxation times ρ_i and angular frequency ω_k as shown in Equation 7.

$$A_{ik} = \frac{\rho_i^2 \omega_k^2}{1 + \rho_i^2 \omega_k^2} \tag{7}$$

An example of the outputs of frequency sweep data modelling is presented in Table 3, where fitting coefficients derived from WLF, CAM and Prony series (used for master curve construction, for pre-smoothing and linear viscoelastic characterization, respectively) are listed at the reference temperature of 10 °C.

WLF coefficients			CAM coefficients			
T_R	C_1	C_2	G_g	ω_c	R	m
°C	-	-	Pa	rad/s	-	-
10	57.88	417.91	10^9	1.27	2.86	0.64

Prony coefficients

i	ρ_i	G_i	i	ρ_i	G_i	i	ρ_i	G_i	i	ρ_i	G_i
-	s	Pa	-	s	Pa	-	s	Pa	-	s	Pa
1	2E-08	4.8E+07	9	2E-04	2.3E+07	17	2E+00	3.4E+06	25	2E+04	9.2E+04
2	6E-08	4.2E+07	10	6E-04	2.3E+07	18	6E+00	2.6E+06	26	6E+04	5.8E+04
3	2E-07	3.5E+07	11	2E-03	1.7E+07	19	2E+01	1.6E+06	27	2E+05	2.9E+04
4	6E-07	4.2E+07	12	6E-03	1.6E+07	20	6E+01	1.2E+06	28	6E+05	1.9E+04
5	2E-06	3.3E+07	13	2E-02	1.1E+07	21	2E+02	6.8E+05	29	2E+06	7.9E+03
6	6E-06	3.7E+07	14	6E-02	9.7E+06	22	6E+02	4.7E+05	30	6E+06	7.0E+03
7	2E-05	2.8E+07	15	2E-01	6.5E+06	23	2E+03	2.6E+05	31	2E+07	8.0E+01
8	6E-05	3.1E+07	16	6E-01	5.3E+06	24	6E+03	1.7E+05	32	6E+07	4.5E+03

Table 3. Example of outputs of WLF, CAM, and Prony coefficients (Bitumen B-PAV).

Once the n Prony terms are defined with the collocation method, the linear viscoelastic response of materials can be depicted in the time domain, by calculating the relaxation modulus G(t) according to Equation 5, and in the frequency domain by deriving the norm and the phase angle of the complex modulus ($|G^*|_{LVE}$ and δ_{LVE}), as indicated in Equations 8 and 9.

$$|G^*|_{LVE} = \sqrt{\left(\sum_{i=1}^{n} \frac{G_i \omega_r^2 \rho_i^2}{\omega_r^2 \rho_i^2 + 1}\right)^2 + \left(\sum_{i=1}^{n} \frac{G_i \omega_r \rho_i}{\omega_r^2 \rho_i^2 + 1}\right)^2} \tag{8}$$

$$\delta_{LVE} = \tan^{-1}\left(\frac{\sum_{i=1}^{n} \frac{G_i \omega_r \rho_i}{\omega_r^2 \rho_i^2 + 1}}{\sum_{i=1}^{n} \frac{G_i \omega_r^2 \rho_i^2}{\omega_r^2 \rho_i^2 + 1}}\right) \tag{9}$$

The agreement between predicted and measured data is graphically illustrated in Figure 3 and 4, where $|G^*|_{LVE}$ and δ_{LVE} computed by Prony series are compared to both pre-smoothened experimental data obtained from the CAM model (Figure 3a and 3b) and measured experimental data (EXP) directly collected from frequency sweep tests (Figure 4a and 4b). From these graphs, where dotted lines represent plot bisectors, it is evident that rheological functions derived from Prony series completely match both pre-smoothened data of $|G^*|_{LVE}$ and δ_{LVE} and measured

experimental data of $|G^*|_{LVE}$. Noticeable deviations were instead found in the case of δ_{LVE} (up to a maximum deviation of 3.7°) when comparing final modelled values to experimental outputs, thus confirming the need to operate a pre-smoothing on raw data and also revealing a better fit of the CAM model to the $|G^*|_{LVE}$ function with respect to δ_{LVE}.
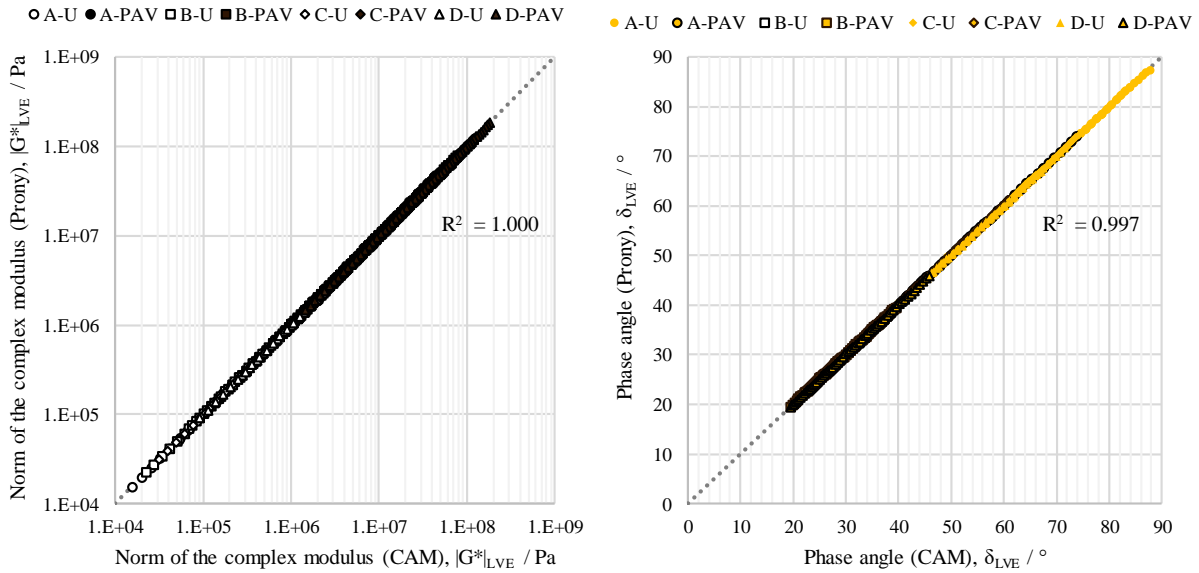

Figure 3. Comparison between rheological parameters predicted from Prony series and pre-smoothened data (CAM) for all materials ($|G^*|_{LVE}$ (a) and δ_{LVE} (b)).
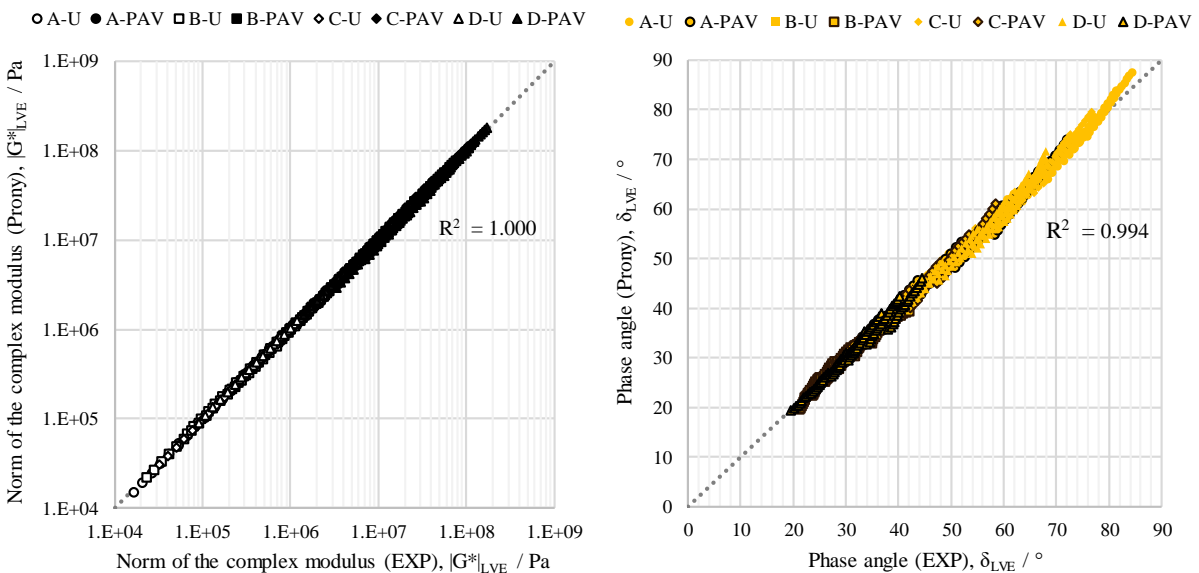

Figure 4. Comparison between rheological parameters predicted from Prony series and measured experimental data (EXP) for all materials ($|G^*|_{LVE}$ (a) and δ_{LVE} (b)).

Outcomes of the linear viscoelastic characterization in the frequency domain are presented in Figure 5, where each plot displays $|G^*|_{LVE}$ and δ_{LVE} of the same bitumen in its unaged and long term aged state.

From a first inspection of the results, remarkable differences can be highlighted among the four binders employed in the experimental study, thus confirming the key role played by crude oil type and production technology on the overall rheological behaviour.

When focusing on the effects of ageing, the norm and the phase angle of the complex modulus were always shifted towards higher and lower values, respectively. This was particularly evident at low reduced frequencies, while in the range of high frequencies a lower influence of ageing was always observed. While these qualitative trends were expected and consistent with typical phenomena taking place in the internal structure of bitumen, it is worth noting that the extent of such changes was substantially different from one bitumen to another even if all binders were subjected to the same ageing history simulated in the laboratory.

The most significant variations were found in the case of bitumen B, with values of the norm of the complex modulus that increased up to 37 times after ageing and relative reductions of phase angle values that reached 46 % in the range of the lowest reduced frequencies investigated. On the contrary, bitumen A exhibited the lowest changes, with values of the norm of the complex modulus after aging that were found to be always lower than 7 times those of the unaged bitumen and relative reductions of the phase angle that were limited to a maximum of 28 %. Binders C and D showed intermediate variations, with a higher impact of the ageing treatments on the linear viscoelastic response displayed by bitumen D, in comparison to C.

Although straightforward correlations between the outcomes of bitumen fractionation and rheology cannot be deduced and a specific trend was not identified, it is interesting to highlight that bitumen B showed the most significant changes after ageing in rheological behaviour and also in the overall colloidal arrangement. This is demonstrated by the highest difference in colloidal

instability index recorded between unaged and aged conditions and in a ratio of asphaltenes to resins that also exceeded unity after ageing (Table 1).

Analysing the extension of master curves along the frequency axis, it can also be observed that ageing affected the time-temperature dependency of binders. All binders showed an increase in the magnitude of the time-temperature shifts after ageing treatments, in line with the outcomes of previous investigation performed on both traditional and innovative bituminous-based binders (Santagata et al., 2012).
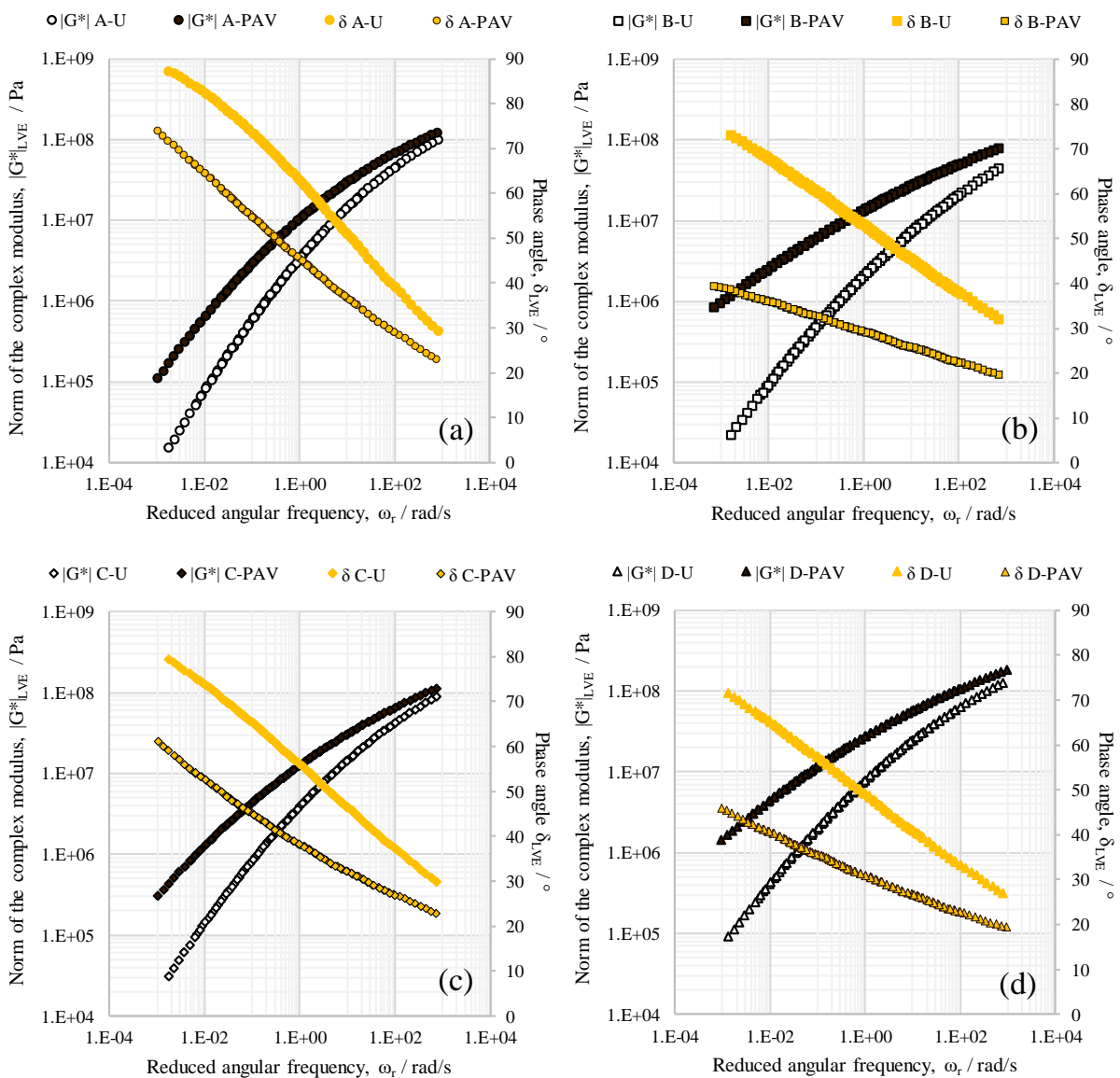

Figure 5. Linear viscoelastic behaviour of bitumen A (a), bitumen B (b), bitumen C (c), bitumen D (d).

Non-linear viscoelastic properties

In order to gain a comprehensive understanding of the response of bituminous binders in typical field conditions, analysis of the viscoelastic properties must be expanded beyond the linear viscoelastic frontier. This is particularly true when considering phenomena that occur in the large strain domain, that make it necessary to discriminate between strain-dependent viscoelastic response and other mechanisms simultaneously taking place in the binder matrix, for example as a consequence of specific damaging processes (Safaei & Castorena, 2017; Underwood, 2016).

Several approaches have been proposed for the assessment of nonlinear viscoelasticity. In the present study, starting from the linear viscoelastic solution, strain-dependent shift factors were derived by means of repeated strain sweep tests, as proposed by Underwood and Kim (2015). A schematic representation of the outputs of a repeated strain sweep test is shown in Figure 6, where the strain input γ and the stress to strain ratio $|G^*|$, normalised with respect to $|G^*|_{LVE}$, are plotted versus time, thus highlighting the typical progression of groups and blocks in a test.
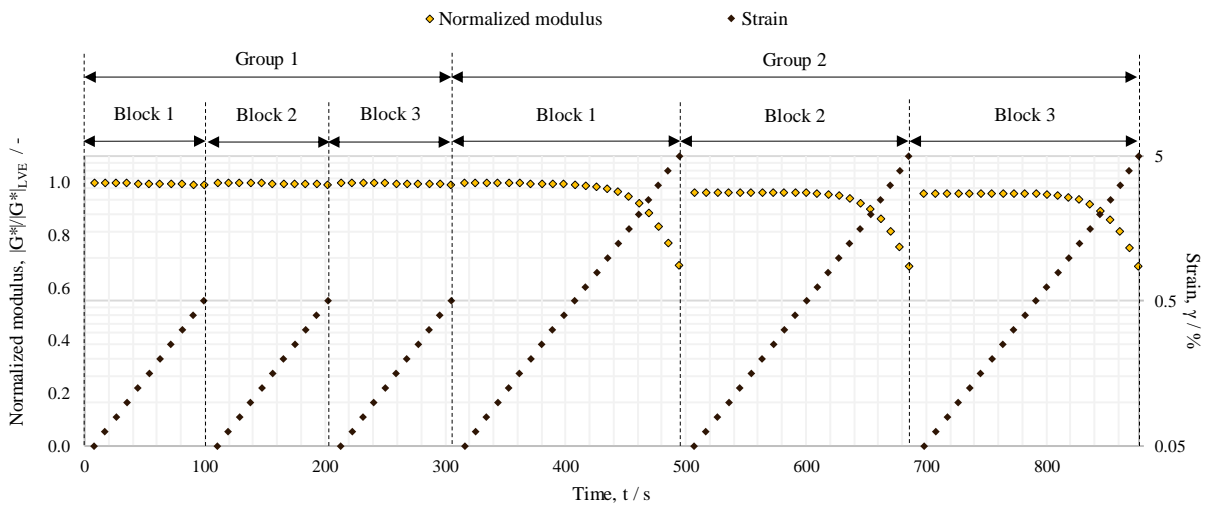
Figure 6. Schematic representation of repeated strain sweep test.

When analysing the plot of normalised modulus versus strain (Figure 7a), it can be noticed that all blocks of group 1 overlap, since the maximum strain in this phase of the test was specifically selected within the linear viscoelastic range. When considering the first block of group 2, the curve initially follows the same path as group 1 curves and then a progressive reduction in

stiffness is recorded until the maximum level of strain is reached. It is postulated that a part of this reduction can be attributed to nonlinearity, while another part is related to other phenomena that, for the purpose of this paper, are generally indicated as damage. While the component of nonlinearity can be considered reversible in the test time-scale, the extent of modulus reduction attributed to damage is considered non-reversible. This hypothesis is supported by the fact that potential self-healing of damage cannot occur if rest period phases are not included between successive blocks. Due to the existence of a component of modulus reduction that cannot be recovered in repeated strain sweep tests, the curve of the second block of group 2 starts from an initial value of normalised modulus that was always found to be lower than that of all previous blocks. Moreover, as a final point at the maximum strain, the curve reached the same modulus recorded during the previous phase (group 2, block 1). The initial reduction in relative stiffness, referred as D in Figure 7, depicts the overall damage accumulated during the first block of the second group. When analysing the third block of the second group, the additional reduction in modulus was found to be minimal. This seems to indicate that the amount of damage remains constant for a specific level of strain and further damage occurring after the first block of a specific group can be considered negligible.

In an attempt to separate the permanent component of damage from nonlinearity, the curve of the second block was vertically shifted of the D quantity, as illustrated in Figure 7b. This shifted curve, that aims at expanding the representation of the viscoelastic response beyond the linear domain, displays the normalised nonlinear viscoelastic modulus ($|G^*|_{NL}/|G^*|_{LVE}$) as a function of strain amplitude. It is interesting to observe that the difference in relative stiffness values found between the shifted curve and the curve of the first block of the second group, reveals how damage accumulates at progressively increasing strain amplitudes during this specific stage of the test. In fact, it can be noted that the two curves follow the same pattern until damage does not affect the response of the material. Then, when damage starts to gradually accumulate within the specimen, a

deviation is observed between the two curves, until the final D value is reached in correspondence of the maximum strain level.
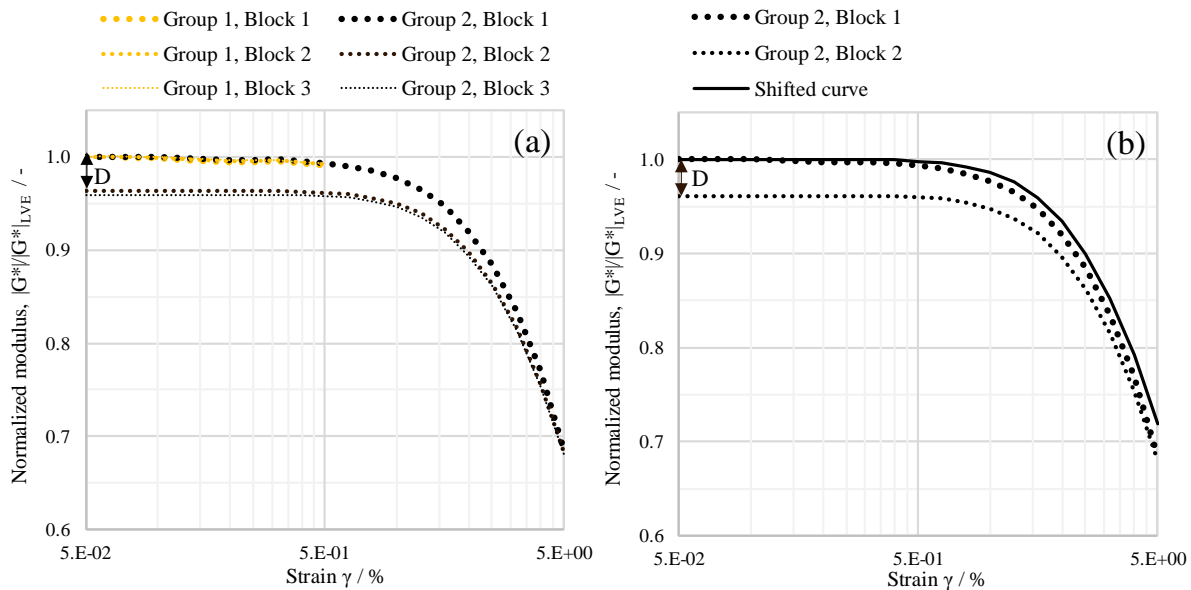

Figure 7. (a) Schematic representation of normalised modulus versus γ during repeated strain sweep tests; (b) Representation of damage subtraction by means of vertical shifting operation.

Nonlinear moduli $|G^*|_{NL}$ were derived for all materials in the temperature (T) and frequency (f) conditions directly investigated by means of repeated strain sweep tests. An example of typical $|G^*|_{NL}(T, f, \gamma)$ curves normalised with respect to $|G^*|_{LVE}(T, f)$ are presented in Figure 8a. It can be noted that curves do not cover the same range of strain amplitudes, since the highest possible strain value that did not lead to an abrupt breakage of the specimen in repeated strain sweep tests depends on both material features and testing conditions. In the present work, the minimum strain amplitude investigated for all binders in all ageing and testing conditions was equal to 5 %.
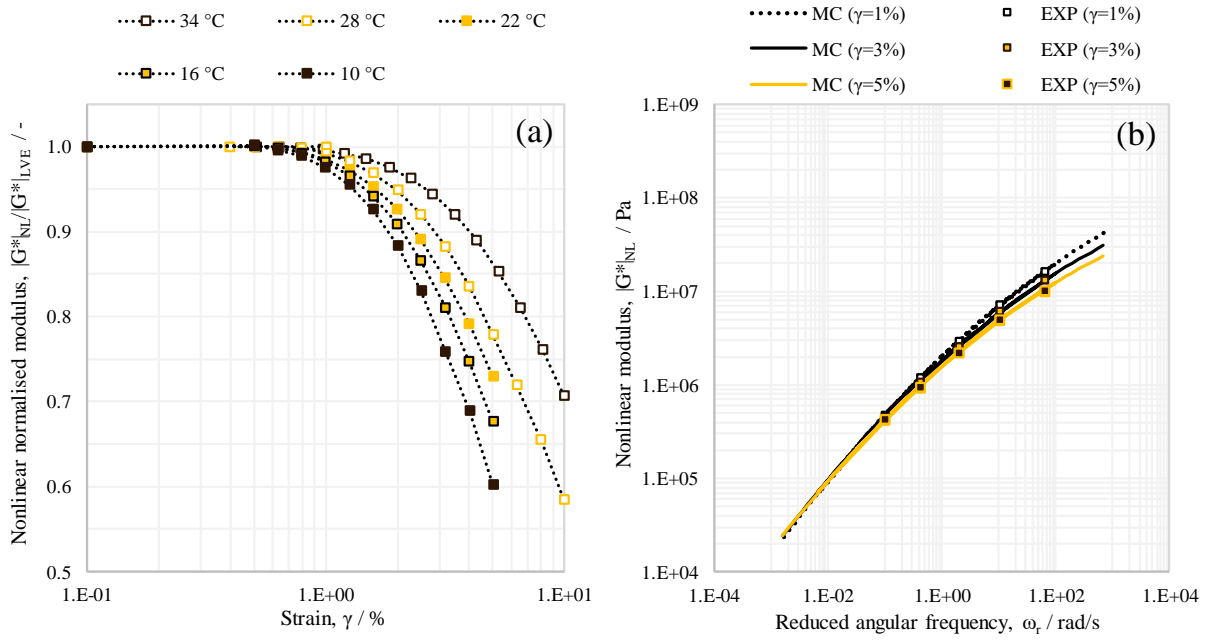
Figure 8. (a) $|G^*|_{NL}/|G^*|_{LVE}$ curves versus γ at different temperatures (bitumen B-U); (b) $|G^*|_{NL}$ master curves (MC) at 1 %, 3 % and 5 % strains using RSS measured experimental data (EXP) at multiple temperatures (bitumen B-U).

Based on the assumption that the time-temperature shift factors are independent of strain, master curves of the nonlinear modulus $|G^*|_{NL}$ were constructed at reference strain levels shifting experimental data measured in repeated strain sweep tests at different temperatures. The strain levels selected for the construction of nonlinear master curves were equal to 0.5 %, 1 %, 2 %, 3 %, 4 %, and 5 %. From an optimization process performed between $|G^*|_{LVE}$ and $|G^*|_{NL}$ master curves, the nonlinear viscoelastic behaviour was modelled from the linear viscoelastic solution by introducing two additional shift factors specifically related to nonlinearity, a_γ and h.

The former represents a horizontal shift that is applied to the reduced frequency with the purpose of changing the logarithmic slope of the LVE master curve, while the latter is a vertical shift that acts on the norm of the complex modulus. This is mathematically described in Equations 10 and 11, where ω_r' is the strain-dependent reduced angular frequency and ω_r is the reduced angular frequency.

$$\omega_r' = \omega_r\, a_\gamma = a_T\, \omega\, a_\gamma \tag{10}$$

$$|G^*|_{NL}(\omega_r) = \frac{1}{h} |G^*|_{LVE}(\omega'_r) \qquad (11)$$

Combining Equations 8 and 10 into Equation 11, $|G^*|_{NL}$ can be calculated by means of Prony series as indicated in Equation 12:

$$|G^*|_{NL} = \frac{1}{h} \sqrt{\left(\sum_{i=1}^{n} \frac{G_i \, \omega'^2_r \, \rho_i^2}{\rho_i^2 \, \omega'^2_r + 1}\right)^2 + \left(\sum_{i=1}^{n} \frac{G_i \, \omega'_r \, \rho_i^2}{\rho_i^2 \, \omega'^2_r + 1}\right)^2} \qquad (12)$$

A comparison between $|G^*|_{NL}$ master curves (at strain levels of 1 %, 3 %, and 5 %) is presented in Figure 8b, where both predicted functions calculated by means of Equation 12 and experimental points measured from repeated strain sweep tests are plotted as a function of the reduced angular frequency.

Inspection of nonlinear shifts can yield a rapid and synthetic description of the impact of nonlinearity on the rheological behaviour of binders. In Figure 9, a_γ and h shifts are plotted as a function of strain for the four binders in the two ageing states. It can be seen that for strain amplitudes approaching zero, both factors tend to unity, thus reducing the nonlinear solution to the reference response in the linear viscoelastic domain.

Either considering the horizontal shift a_γ or the vertical shift h, the lowest deviation from the linear response was showed by bitumen A, followed by bitumens C, D, and B. This ranking was found to be the same in both the unaged and long-term aged conditions and, interestingly, it also reflects the trend found when the sensitivity to ageing in the linear viscoelastic domain was analysed.

By focusing on the effects of ageing on the nonlinear viscoelastic response, it is worth noting that nonlinear shifts always increased after ageing. This outcome seems consistent with association and polymerization mechanisms that typically take place during ageing. The higher strain-dependency can be explained by considering that the increased dimensions and/or increased number of units of rigid asphaltenes particles can exacerbate stretching phenomena experienced by the maltene phase of bitumen.

The ratio of the shift factor values after ageing to those in the unaged state were found to linearly increase with the strain level, with no substantial differences among different materials. This finding suggests that the impacts of ageing on the strain dependency of free energy and entropy production are relatively consistent across binders (Underwood and Kim, 2015). The only exception was found in the case of bitumen B, that exhibited a different trend and the overall highest variations in the nonlinear shift factors after ageing. The precise reasons for the peculiar behaviour of this bitumen is unknown and its investigation is beyond the scope of the current work. However, it is noted that bitumen B had the greatest increases in both CII and As/Re indices from ageing.
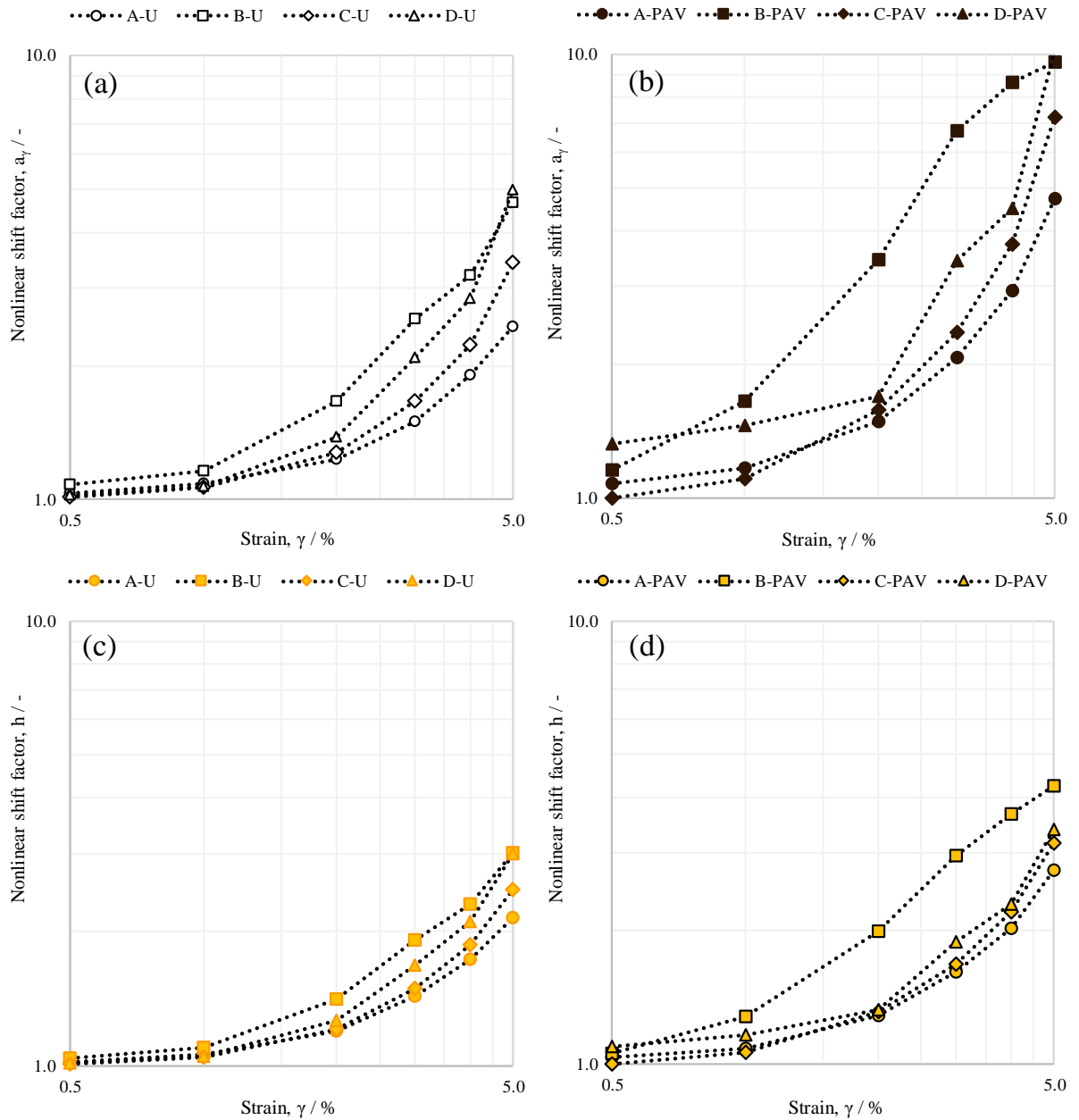
Figure 9. Nonlinear shift factors: (a) a_γ versus γ for unaged binders, (b) a_γ versus γ for aged binders, (c) h versus γ for unaged binders, (d) h versus γ for aged binders.

Conclusions

Based on the outcomes of the experimental investigation presented in this paper, it can be concluded that the adopted testing and modelling approach can be an effective tool for assessing the viscoelastic properties of bituminous binders and the influence of chemical ageing in both the linear and nonlinear domains.

With regard to linear viscoelasticity, ageing affected the time-temperature dependency of binders and induced an expected increase in stiffness and elasticity that was particularly evident in the range of low frequencies and/or high temperatures. In the nonlinear domain, an intensification of the strain-dependent behaviour was always exhibited, as demonstrated by the increase in nonlinear shift factors and by the progressive contraction of the linear viscoelastic range after ageing. These findings revealed univocal trends that were coherent with permanent changes occurring in the bitumen microstructure as a consequence of ageing. Moreover, it is worth noting that the magnitude of such changes was found to be strictly dependent on material features, thus proving that crude source and manufacturing process strongly impact on the susceptibility of bitumen to chemical ageing. With specific reference to the SARA analysis results, fractionation indicators were found to be consistent with the viscoelastic response exhibited in both the linear and nonlinear domains. Deeper investigations as to the precise chemical or structural origins of these behaviours requires further analyses. Moreover, future studies will focus on the definition of specific shift factors capable of taking into account the effects of ageing in viscoelastic modelling.

References

Airey, G.D. (2002). Use of black diagrams to identify inconsistencies in rheological data. *Road Materials and Pavement Design, 3(4),* 403-424.

Airey, G.D. (2003). State of the art report on ageing test methods for bituminous pavement materials, *International Journal of Pavement Engineering 4 (3),* 165-176.

Hofko, B., Porot, L., Falchetto Cannone, A., Poulikakos, L. Huber, L., Lu, X., Mollenhauer, K., & Grothe H. (2018). FTIR spectral analysis of bituminous binders: reproducibility and impact of ageing temperature, *Materials and Structures 51:45*.

Lesueur, D. (2009). The colloidal structure of bitumen: Consequences on the rheology and on the mechanisms of bitumen modification. *Advances in Colloid and Interface Science, 145,* 42-82.

Lu, X., & Isacsson, U. (2002). Effect of ageing on bitumen chemistry and rheology. *Construction and Building Materials, 16*, 15-22.

Fallah, F., Khabaz, F., Kim, Y-R, Kommidi, S.R., Haghshenas, H.F. (2019). Molecular dynamics

modeling and simulation of bituminous binder chemical aging due to variation of oxidation level and saturate-aromaticresin-asphaltene fraction. *Fuel, 237*, 71-80.

Ferry, J.D. (1980). Viscoelastic properties of polymers, John Wiley and Sons.

Glover, J. C., Epps Martin, A., Chowdhury, A., Han, R., Prapaitrakul, N., Jin, X., & Lawrence, J. (2009). Evaluation of binder aging and its influence in aging of hot mix asphalt concrete: literature review and experimental design. Report FHWA/TX-08/0-6009-1, Texas Transportation Institute, College Station, TX.

Marasteanu, M.O., & Anderson, D.A. (1999). Improved model for bitumen rheological characterization. Proceedings of the Eurobitume Workshop on Performance Related Properties for Bituminous Binders, 1-4.

Masad, E., Huang, C.W., Airey G., & Muliana, A. (2008). Nonlinear viscoelastic analysis of unaged and aged asphalt binders. *Construction and Building Materials, 22,* 2170-2179.

Mirwald, J., Maschauer, D., Hofko ,B. , Grothe H. (2020). Impact of reactive oxygen species on bitumen aging – The Viennese binder aging method. *Construction and Building Materials, 257,* 119495.

Paliukait, M., Vaitkus, A., Adam Zofka, A. (2014). Evaluation of bitumen fractional composition depending on the crude oil type and production technology, The 9th International Conference on Environmental Engineering, Vilnius, Lithuania.

Petersen, J. C. (1986). Quantitative Functional Group Analysis of Asphalts Using Differential Infrared Spectrometry and Selective Chemical Reactions – Theory and Application. *Transportation research record 1096.*

Rahmani, E., a, Darabi, M. K., Little, D. N., & Masad, E. A. (2017). Constitutive modeling of coupled aging-viscoelastic response of asphalt concrete. *Construction and Building Materials, 131,* 1-15.

Safaei, F., Castorena, C. (2017). Material nonlinearity in asphalt binder fatigue testing and analysis. *Materials and Design, 133,* 376-389.

Santagata, E., Baglieri, O., Tsantilis, L., & Dalmazzo, D. (2012) Rheological Characterization of Bituminous Binders Modified with Carbon Nanotubes. *Procedia, Social & Behavioral Sciences,* 546-555. ISSN: 1877-0428.

Siddiqui, M. N., & Ali, M. F. (1999). Studies on the ageing behavior of the Arabian asphalts. *Fuel, 78,* 1005-15.

Sun, X., Qin, X., Zhisheng Liu, Z., Yin, Y., Zou, C., Jiang, S. (2020). New preparation method of bitumen samples for UV aging behavior investigation, *Construction and Building Materials, 233,* 117278.

Tauste, R., Moreno-Navarro, F., Sol-Sánchez, M., & Rubio-Gámez M. C. (2018). Understanding the bitumen ageing phenomenon: A review. *Construction and Building Materials*, 192, 593-609.

Underwood, B. S. (2016). A continuum damage model for asphalt cement and asphalt mastic fatigue. *International Journal of Fatigue, 82,* 387-401.

Underwood, B. S. & Kim, Y. R. (2015). Nonlinear viscoelastic analysis of asphalt cement and asphalt mastics. *International Journal of Pavement Engineering 16:6,* 510-529.

Walubita, L.F., A.E. Martin, S.H. Jung, C.J. Glover, & E.S. Park. (2006). Application of Calibrated Mechanistic Fatigue Analysis with Aging Effects. Report FHWA/TX-06/0-4468-3, Texas Transportation Institute, College Station, TX.